Rheology of water in small nanotubes

Jose Cobeña-Reyes and M. Sahimi*
Mork Family Department of Chemical Engineering and Materials Science, University of Southern California, Los Angeles, California 90089-1211, USA

(Received 12 April 2020; accepted 20 July 2020; published 10 August 2020)

The properties of water in confinement are very different from those under bulk conditions. In some cases the melting point of ice may be shifted and one may find either ice, icelike water, or a state in which freezing is completely inhibited. Understanding the dynamics and rheology of water in confined media, such as small nanotubes, is of fundamental importance to the biological properties of micro-organisms at low temperatures, to the development of new devices for preserving DNA samples, and for other biological materials and fluids, lubrication, and development of nanostructured materials. We study rheology and dynamics of water in small nanotubes using extensive equilibrium and nonequilibrium molecular dynamics simulations. The results demonstrate that in strong confinement in nanotubes at temperatures significantly below and above bulk freezing temperature water behaves as a shear-thinning fluid at shear rates smaller than the inverse of the relaxation time in the confined medium. In addition, our results indicate the presence of regions in which the local density of water varies significantly over the same range of temperature in the nanotube. These findings may also have important implications for the design of nanofluidic systems.

DOI: 10.1103/PhysRevE.102.023106

I. INTRODUCTION

Water, in addition to being vital for life, is one of the most intriguing fluids, as many of its properties exhibit anomalous behavior. For example, its density reaches its maximum at 277 K. The anomalous behavior of several of water's other properties is enhanced as the temperature T decreases [1]: its isothermal compressibility increases as T decreases, reaching a maximum, and then it decreases [2] at still lower temperatures. Under supercooled condition, water density reaches a minimum at around 203 K [3], while its heat capacity reaches a maximum near 250 K [4], and its thermal conductivity attains a maximum at about 400 K [5]. Such intriguing anomalies at low temperatures have given rise to fundamental questions, which is why it is not surprising that numerous theoretical and experimental studies, as well as computer simulations, have been undertaken in order to understand the behavior of water over a wide range of temperature.

Compared with bulk liquid water, confined water at room temperature exhibits stronger anomalies. For example, it is well known that self-diffusion of water strongly decreases upon confinement [6–14], and that the dynamics of the system slows down [15–18]. Similarly, water's thermodynamic properties may be altered. In the past, it was reported, based on molecular dynamics (MD) simulations, that the water phase diagram can develop a "shift" when affected by confinement [19]. Later on, a phase diagram was proposed [20] that indicated a decrease in the melting point. Furthermore, different liquid phases, such as low- and high-density liquid, have been reported in carbon nanotubes (CNTs) [21], even at room temperatures. There is also evidence for a possible second critical point below the freezing point, where the three phases can coexist [22,23].

Below freezing temperature, confinement may lead to inhibition of freezing and a deeply cooled liquid state [24], giving rise to even more anomalous properties than under bulk conditions. Water is no exception and, indeed, analyzing the behavior of supercooled water in confined media below the bulk freezing temperature of 273 K reveals very intriguing phenomena [24–27]. We recently showed [28,29] that water in small CNTs and their silicon-carbide counterparts [silicon-carbide nanotubes (SiCNTs)] of a specific size does not freeze, even below 231 K, the temperature for bulk homogeneous nucleation [30]. Inhibiting freezing inside small tubes or pores may be accomplished, if their diameter is smaller than a critical size of about 3–4 nm [31]. Similarly, by calculating the mean-squared displacements (MSDs) of the molecules in CNTs, it was determined that 8.6 Å is the critical radius in which freezing is repressed [32]. It was also demonstrated [10] that in both CNTs and SiCNTs the Stokes-Einstein relation between the viscosity and diffusivity is no longer satisfied, and that temperature dependence of the self-diffusivity indicates a transition from a fragile to a strong liquid state at 230 K. Understanding the anomalous behavior of water under such conditions is highly relevant to many chemical, biological, and physical phenomena [33], including the question of how micro-organisms survive at very low temperatures, development of new instruments for preserving DNA, lubrication problems, and fabrication of nanomaterials [34,35].

Another common phenomenon in water flow in nanotubes is the slip boundary condition on the nanotubes' walls. In addition, Ramos-Alvarado *et al.* [36] studied water-silicon interactions and reported that the contact angle can be used to predict the slip length. Similarly, Wei *et al.* [37] reported that

*moe@usc.edu

functionalization of confined media can weaken or strengthen the slip velocity, which is usually orders of magnitude larger than what is predicted by the Hagen-Poiseuille (HP) (laminar) flow in tubes. Atomistic composition of the confined media can, in fact, drastically change the contact angle and the slip velocity, produce very fast flow in hydrophilic materials, and in hydrophobic media make the layer next to the wall either slip or stick to it; it can, of course, also be adsorbed there [38].

The anomalous behavior of water in nanotubes has also been reported in other types of nanostructured materials, such as self-assembled nanolayers (SAMs) that are important to biological and tribological applications. Lorenz *et al.* [39], for example, found that even when the diffusion coefficient of water increases up to two orders of magnitude when confined between layers of alkylsilane-SAMs no ice layers were found (although even hydrocarbons exhibit layered structures under confinement [40]), which is different from what happens in nanotubes where icelike behavior and layering is observed. Nonetheless, Ramin and Jabbarzadeh [41] reported that water does behave in an icelike fashion when it is confined under high pressures in other types of SAMs, such as *n*-alkanethiols, implying that despite confinement of the SAM structure the formation of icelike structures depends not only on the thermodynamics of the system but also on the atomistic composition of the nanostructured materials.

Due to the complex interactions between the water molecules, as well as between them and a confined medium's walls, use of MD simulation is imperative. Studies involving confined water in isolated nanotubes require, however, special treatment regarding the equilibration time. For example, when the molecular structure of water is represented by such models as the SPC/E and TIP4P/ice, the melting point cannot be reached in less than 10 ns [42] of MD simulation. Moreover, the motion and arrangement of the molecules can produce false crystalline structures, which are products of the artifacts caused by periodicity [43] of the simulation cell, or when the Ewald summation method or the particle-particle-particle-mesh (PPPM) approach is used to compute the electrostatic interactions, but the implementation of the method is not done properly, which can lead to inaccuracies in the computed properties, as demonstrated by Bostick and Berkowitz [44].

Viscosity of fluids is usually computed by either the Green-Kubo (GK) method or by nonequilibrium MD (NEMD) simulation. Both are computationally expensive, due to the necessity of requiring long simulations to generate enough fluctuating samples in the GK method, or because of the requirement in the NEMD simulation that one must achieve steady state that is usually reached on a time scale t that is related to the viscoelastic relaxation time of the fluid, which can be quite long. Assuming that water is a Newtonian fluid allows use of the equations that are used in the bulk regime or in large tubes. It was shown recently, however, that the velocity profile of water or other Newtonian fluids flowing in nanotubes is not necessarily parabolic (the HP flow), even when the Reynolds number was low enough [38]. This affects directly computation of the shear rate and shear stress in nanotubes, disallowing use of the equations for Newtonian fluids in the HP regime. Indeed, we are not aware of any study in which the rheology of supercooled water in nanotubes, and in particular its shear stress versus shear rate diagram, has been measured or computed. Other physical quantities, such as the intermediate scattering function, help computing the relaxation time that is related to the viscosity [45]. Nonetheless, in supercooled liquids the shear-thinning behavior occurs at shear rates several orders of magnitude smaller than the inverse of the relaxation time [46,47]. It should also be noted that the shear-thinning rheology can be observed in any bulk liquid, as long as the applied shear rate is greater than a critical shear rate $\dot{\gamma}_c$.

Given the anomalous behavior of water over a wide range of temperatures, its rheology is also important, but has remained unexplored. The goal of the present paper is to study the dynamics and rheology of water in small nanotubes over a wide range of temperature, using extensive MD simulations. As described below, our results indicate interesting and important rheological behavior for water.

The organization of the rest of this paper is as follows. We first describe the molecular model of the nanotubes and the details of the molecular simulations. The results are then presented and discussed, including the basis for suppression of freezing of water confined in a nanotube by computing some of the characteristic quantities. To study the rheology of confined water, we compute the shear rate and the viscosity using a NEMD method that does not assume any specific velocity profile for the water, and compare the results with those computed by the GK equation, as well as with the shear viscosity of bulk water. We then discuss the differences between the bulk and confined critical shear rates, and their relation with the relaxation time computed by the ISF. The paper is summarized in the last section.

II. MOLECULAR MODELS AND COMPUTATIONAL METHODS

We first describe the molecular model of the nanotube that we employed in the simulations, after which we explain the computational procedure and the quantities that we have computed for the bulk and confined water.

A. The nanotubes

We used a SiCNT as the model of confined media but, as we demonstrated recently [28], the same type of phenomena and results that we present in this paper is also obtained in carbon nanotubes. It is, of course, well known that SiC has exceptional properties, such as thermal and mechanical stability up to very high temperatures, as well as high thermal conductivity [48]. In the past we utilized SiC for fabricating nanoporous membranes [49] for hydrogen separation at high temperatures in a very corrosive environment, and fabricated SiCNTs as potential materials for hydrogen storage [50–52]. Others have used SiC membranes for biomedical applications [53], and studied it [54] as material for storage of natural gas. In the present paper we used three single-wall SiCNTs, namely, the (12,0), (20,0), and (30,0) tubes with diameters $D = 11.9,\ 19.9$, and 29.8 Å. Note that among all the possible SiCNT structures those with equal numbers of C and Si atoms were shown [55] to be most stable, which is also the type that we use. In setting the nanotube's length ℓ, one should take into account the well-known fact [56] that the MSDs in a confined

medium are influenced by finite-size effects. Thus, to set ℓ we first computed the MSDs of the oxygen along the axial direction z,

$$\langle \Delta^2 z(t) \rangle = \frac{1}{N} \sum_{i=1}^{N} [z_i(t) - z_i(0)]^2, \tag{1}$$

for various lengths of the nanotube, where N is the total number of oxygen atoms, taking into account the change in the center of mass when computing the MSDs. While there were indeed finite-size effects, we found that for lengths $\ell =$ 300, 250, and 160 Å of, respectively, the (12,0), (20,0), and (30,0) nanotubes the finite-size effects were negligible. Thus, we set the nanotubes' lengths at $\ell = 325$, 300, and 180 Å. Note that the length of the C-Si bond is 1.8 Å [57].

B. Computational protocol for bulk water

A cubic simulation cell of linear size $L = 35$ Å was filled up with 1331 water molecules, represented by the TIP4P/ice [58] model, which predicts a bulk freezing point of 271.3 K. The initial density was 0.93 g/cm^3 at $T = 230$ K and $P =$ 1 atm, taken from a recent model that predicts the density of supercooled water [59]. Equilibrium MD (EMD) and the NEMD simulations were carried out for, respectively, 10 and 50 ns. Such long simulations are required for computing the relaxation time using the ISF by the EMD simulations, and to attain steady state when very low shear rates are simulated in the NEMD calculations. The NPT ensemble was used for the equilibration of the system at pressure $P = 1$ atm. After 10 ns of equilibration the Nosé-Hoover thermostat was used in the production stage of the MD simulations, whereas the algorithm based on the SLLOD equation of motion[1] was employed in the NEMD [60]. The self-part of the ISF was computed using

$$F_s(\boldsymbol{\kappa}, t) = \frac{1}{N} \left\langle \sum_{j=1}^{N} \exp\{-i\boldsymbol{\kappa} \cdot [\mathbf{r}_j(t) - \mathbf{r}_j(0)]\} \right\rangle, \tag{2}$$

where $\mathbf{r}_j(t)$ is the position vector of atom j at time t, and $\langle \cdot \rangle$ implies an ensemble average. We computed the ISF for the hydrogen atoms, as they have a larger scattering area. $F_s(\kappa, t)$ is typically fitted to a stretched exponential function, also known as the Kohlrausch-Williams-Watts function [61,62]:

$$F_s(\boldsymbol{\kappa}, t) = a \exp[-(t/\epsilon)^{\beta}], \tag{3}$$

in which ϵ is the relaxation time, and a and β are constants. In the NEMD simulation the shear viscosity was computed using

$$\eta = -\frac{\tau_{xy}}{\dot{\gamma}}, \tag{4}$$

where τ_{xy} is the shear stress, and $\dot{\gamma}$ is the shear rate. We used a wide range of the shear rates in order to identify the onset of non-Newtonian behavior of water, if any.

[1]The name SLLOD is due to the use of the transposed Doll's tensor, the dyadic product of the positions and momenta, which was named after the Kewpie Doll by Hoover.

C. Computational protocol for confined water

After inserting the (12,0), (20,0), and (30,0) nanotubes in individual simulation boxes with linear dimensions of, respectively, 400, 350, and 240 Å, water molecules were distributed in the box, including in the nanotube, with a density of 1 g/cm.^{3} The SiCNTs were modeled by the Tersoff [63] potential that has been widely used for estimating the mechanical properties of SiCNTs [56,64–67]. The interactions between water and the SiCNTs were represented by the Lennard-Jones (LJ) potential, the parameters of which for the SiCNTs were taken from Malek and Sahimi [50], while the partial charges were taken from the *ab initio* calculations reported previously [55]. The Lorentz-Berthelot mixing rules were employed to compute the LJ parameters of pairs of atoms.

The energy of the system was then minimized, which typically took between 1.5 and 3 ns. Then, EMD simulations were carried out at each temperature in the NVT ensemble for 10 ns in order to allow the water molecules to move in and out of the nanotubes. After equilibrium was reached, water molecules outside the nanotube were removed, the axis of the simulation box was aligned with that of the nanotubes, and periodic boundary conditions were imposed. The system was then taken to its final temperature. We also ran a set of simulations in the (12,0) SiCNT at 80 and 290 K in order to visualize solid and liquid states on both sides of the freezing point.

After the structures were generated, separate sets of MD and NEMD simulations for each case were carried out. The EMD simulations were done for 10 ns to compute the cage correlation function (CCF), the MSDs, and the radial distribution function (RDF) $g(r)$ at several temperatures. Calculation of the ISF, however, required 200 ns to reach its low values. In order to analyze the local density fluctuations of water, we used the Voronoi tessellation method to compute the volume occupied by the molecules. The local density of water is given by its mass divided by the volume of the Voronoi blocks in which it resides. Then, a local density larger than 1.0 g/cm^3 was considered as the high; if it was between 0.9 and 1.0 g/cm^3, it was labeled as normal density, whereas a density less than 0.9 g/cm^3 was viewed as the low. Based on such classification, we analyzed the local density fluctuations of water in the nanotube.

To compute $C(t)$, the CCF, we used a generalized neighbor list [68] in order to keep track of the locations of neighbors of every molecule, using the first solvation shell as the boundary, since we wish to understand how fast the cage rearranges itself. If $C(t) = 1$, the list for any atom at time t remains unchanged relative to time $t = 0$. If, however, a molecule diffuses outside its surrounding cage, the lists at times t and $t = 0$ will not be identical, and $C(t) = 0$ at time t. Thus, $C(t)$ was computed by averaging over all the atoms in the nanotube. We used the location of the oxygen atoms as the basis for calculating $C(t)$, because it is the closest to the center of mass of H_2O. The aforementioned list was represented by a vector of neighbors of each individual oxygen atom i in the CNT with radial distance r_{list}:

$$\mathbf{L}_i(t) = [f(r_{ij})], \quad j = 1, 2, \ldots, N, \tag{5}$$

where N is the total number of atoms in the system, and

$$f(r_{ij}) = \begin{cases} 1 & r_{ij} \leqslant r_{\text{list}} \\ 0 & \text{otherwise.} \end{cases} \tag{6}$$

We used a cutoff $r_{\text{list}} = 3.25$ Å, which is the lowest value of the first well in the RDF. Using a larger value of r_{list} may lead to misinterpreting the results. Then, $C(t)$ is given by

$$C(t) = \frac{\langle \mathbf{L}_i(0) \cdot \mathbf{L}_i(t) \rangle}{\langle \mathbf{L}_i^2(0) \rangle}. \tag{7}$$

The MSDs in the axial direction z were computed through Eq. (1). The zero shear rate viscosity was computed using the GK equation, by integrating the stress-stress autocorrelation function of the three off-diagonal entries of the viscous pressure tensor:

$$\eta(T) = \frac{V}{3k_BT} \int_0^\infty [\langle \tau_{xy}(t)\tau_{xy}(0) \rangle + \langle \tau_{xz}(t)\tau_{xz}(0) \rangle + \langle \tau_{yz}(t)\tau_{yz}(0) \rangle] dt, \tag{8}$$

where V is the volume of the system, and k_B is Boltzmann's constant.

The NEMD simulations were carried out for between 10 and 20 ns. At time $t = 0$ an axial force was applied to every water molecule in order to induce motion. To do so, the z-axis (axial) degree of freedom was removed from the thermostat to avoid artificial heating of the system. It took about another 8 ns for the systems to reach steady state. Once the velocity of the center of mass of water molecules reached steady state, the external applied force was turned off to allow water molecules to decelerate. Computation of the deceleration could have been done by various ways. Here, however, we only used up the 800 fs right after the external force was removed to avoid inaccuracies due the motion of the z-axis degree of freedom of the thermostat. Such approach has been used before in several studies of confined water [69–74]. Data for the velocities were collected every 1 fs, and averaged over 5-fs intervals, where the average was defined by $\bar{v} = M^{-1} \sum_i^N m_i v_i$, with M being the total water mass in the tube, m_i and v_i the mass and velocity of water molecule i, and N the total number of water molecules.

To compute the quantities of interest, we proceeded as follows. After removing the external force, the deceleration $\bar{a}$ of the water molecules was computed. Then, the shear stress at the wall was calculated by

$$\tau = \frac{M\bar{a}}{\pi DL}, \tag{9}$$

which is obtained by a force balance and is independent of the rheology. Note that because the LJ cutoff was set at 12, 20, and 30 Å for the three nanotubes, which are slightly larger than each nanotube's diameter, all water molecules interact with the walls. Thus, Eq. (9) is representative of the shear stress in the nanotube. We also point out that Eq. (9) does not contain a pressure term, because the force applied to each particle to induce flow was used. To compute the shear rate $\dot{\gamma}$, we divided the interior of the nanotube into five concentric cylinders, the maximum number of layers in which the water molecules were distributed in the tube. The center-of-mass velocity for the groups was used for computing the mean shear rate, given by

$$\gamma = \left\langle \left(\frac{\partial V_z}{\partial r} + \frac{\partial V_r}{\partial z} \right) \right\rangle. \tag{10}$$

Thus, since $\partial V_r/\partial z \approx 0$, we have

$$\gamma = \left\langle \frac{\partial V_z}{\partial r} \right\rangle \approx \left\langle \frac{\Delta V_z}{\Delta r} \right\rangle, \tag{11}$$

where $\Delta V_z/\Delta r$ denotes the difference in the values between two layers at a distance Δz. Finally, the average shear rate was computed using those obtained by Eq. (11). Multiple values of the applied force were employed to simulate water flow in the nanotubes over a wide range of the fluid velocities. Note that the pressure component $P_{zz} = 1$ atm in the simulations.

Let us point out that, due to slip on the nanotube's wall, computing the shear rate is a difficult problem, and particularly so if its value is small. For example, it was not possible to compute the shear rate at velocities v_z smaller than 10 m/s, which are velocities that are comparable with the thermal velocities of the molecules. Moreover, the water layers in the nanotube may have velocities that are close to each other. To overcome this difficulty, the velocity of the center of mass of each layer was averaged over all the time between the beginning of the steady-state velocity profile and the time at which the external force was removed. This removed most of the thermal noise, making it possible to obtain accurate results. In addition, a minimum of 30 realizations were generated for each data point to improve the statistics, and for velocities smaller than $v_z = 30$ m/s at least 50 realizations were used.

In both the EMD and NEMD simulations, long-range Coulombic interactions were computed by the PPPM method [75]. The SHAKE algorithm [76] was used to keep the bonds and angles in the water molecules intact. Temperature was adjusted by the Langevin thermostat, and its increase to higher values, when needed, was done at a rate of 1 K after every 5 ps. All the simulations were carried out using the LAMMPS package [77], and the systems were visualized using the VMD package [78]. The time step was always 1 fs. As mentioned earlier, water molecules were represented by the TIP4P/ice [58] model. Their viscosity at 273 K, calculated by the TIP4P/ice model, is 1.78 cP [79], which is larger than the experimental value of 1 cP, but is of the correct order of magnitude.

III. RESULTS AND DISCUSSION

We computed several important physical quantities that characterize the rheology and dynamics of supercooled water in small nanotubes. In what follows we present and discuss them.

A. The cage correlation function and mean-squared displacements

Figure 1 presents the CCF at three widely disparate temperatures. At 80 K the CCF does not change, indicating a frozen state. It decays clearly at 230 K, indicating that the cage formed by the water molecules rearranges itself continuously due to jumping of the molecules into a different cage. The decay of the CCF is the sharpest at 290 K, as expected.

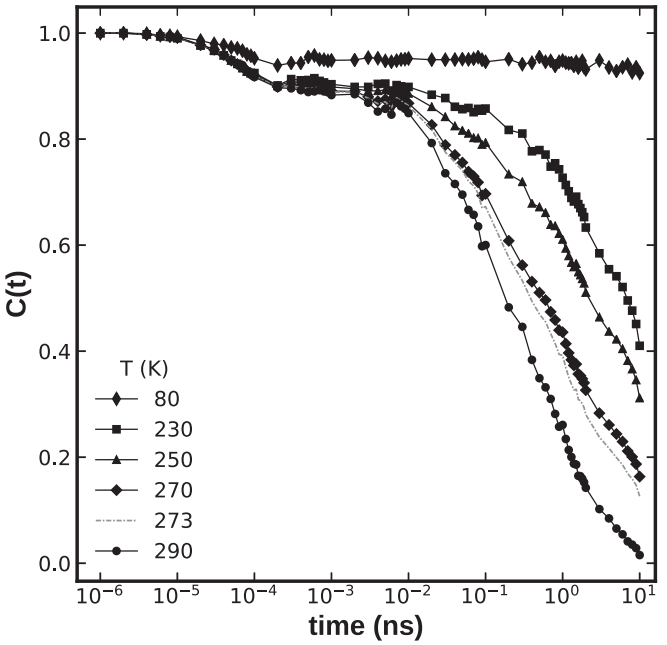

FIG. 1. The cage correlation function $C(t)$. The results at 80 K indicate a frozen state, whereas those at other temperatures are representative of a liquid state.

Figure 2 presents the results for the MSDs. They are practically zero at 80 K, not changing over time. But, they grow continuously with the time at 230 K and higher temperatures. Moreover, at longer times the MSDs vary essentially linearly with the time, indicating ordinary diffusive motion. The inset in Fig. 2 shows the diffusion coefficient D, computed based

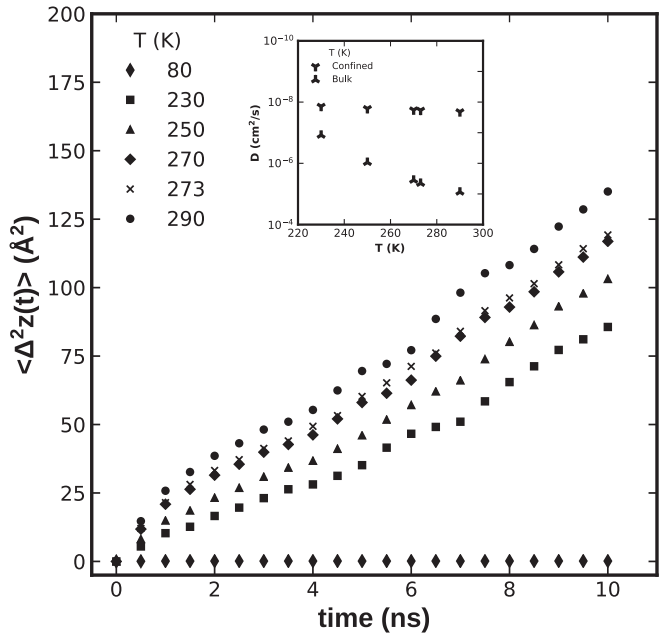

FIG. 2. Axial mean-squared displacements $\langle \Delta^2 z(t) \rangle$ of water. The results at 80 K indicate a frozen state. The inset compares the diffusivities in confinement with the bulk values. The bulk values were taken from Ref. [80].

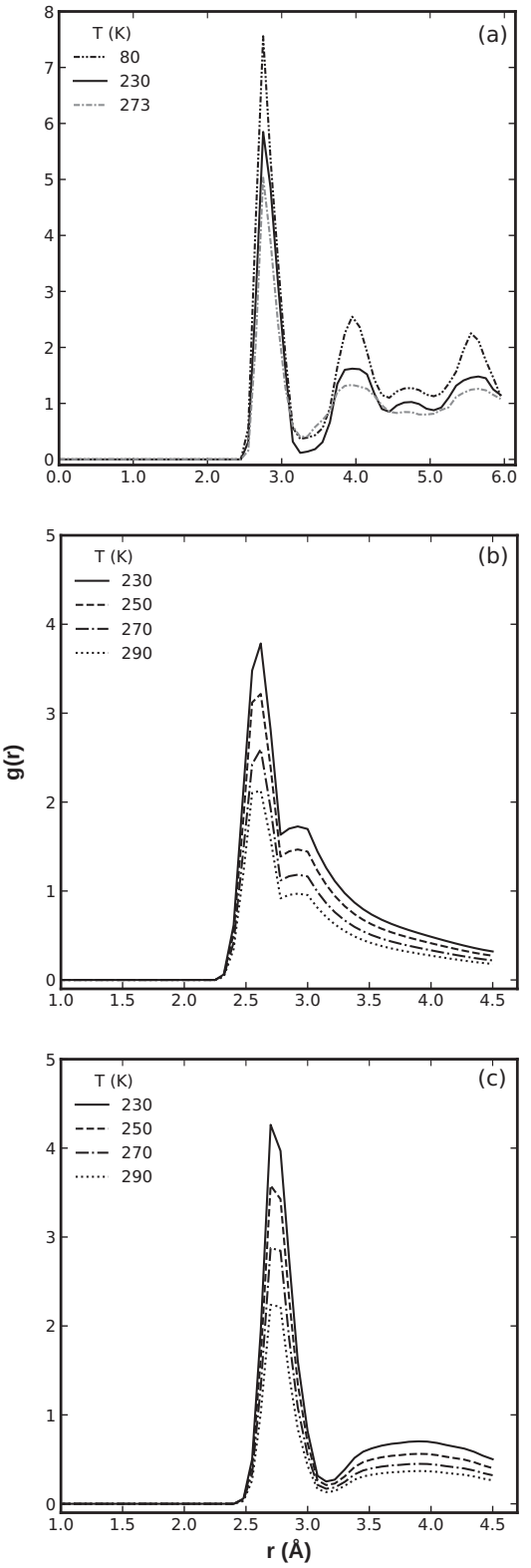

FIG. 3. The radial distribution function $g(r)$, which provides evidence for a (a) liquid state, and the existence of (b) low- and (c) high-density water regions in the (12,0) nanotube.

on the MSDs. The bulk values were taken from Ref. [80]. The results in Figs. 1 and 2 are completely consistent with the existence of a liquid state below the bulk freezing temperature.

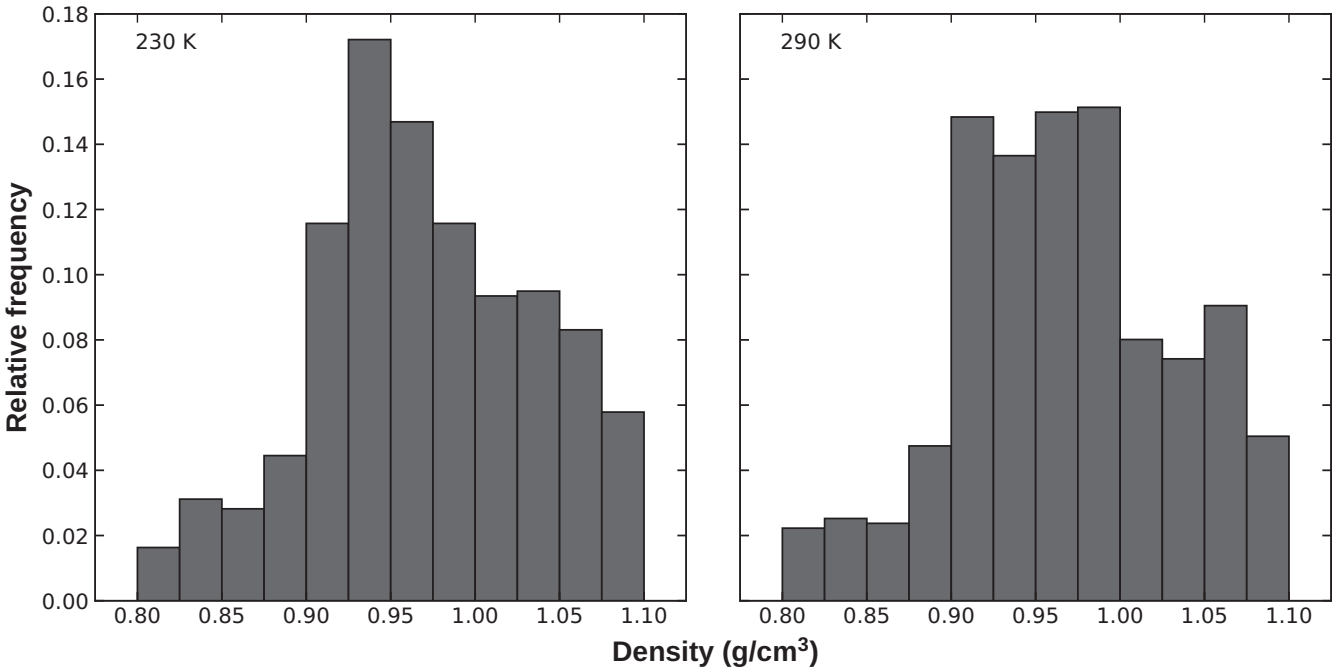

FIG. 4. Histogram of density fluctuations of water in the (12,0) nanotube.

B. Radial distribution function and density fluctuations of liquid water

The radial distribution function $g(r)$ of the oxygen-oxygen pairs is shown in Fig. 3(a). The differences in the relative heights of each peak at $T = 80$ and 230 K are consistent with the results shown in Figs. 1 and 2. The second and third peak at 230 K are more "flat," when compared with those at 80 K, indicating that at 230 K one has a liquid state.

The presence of the three types of density was confirmed by the computation using the Voronoi volumes, as described earlier, as well as the RDF $g(r)$. Locally low and high densities have distinct $g(r)$ patterns. This is shown in Fig. 3. For high density the second peak collapses, with the first one leaving a small shoulder at $r \approx 3$ Å. Moreover, the first peak corresponding to the high density develops before the first peak representing the low density, which is due to the closeness of the water molecules in the former region. The second peak corresponding to the low densities is broad and larger than the corresponding one in the region with high density, due to the larger probability of finding water molecules than in the latter.

At 230 K the normal density water tends to occupy the largest portion among the three, representing about 55% of the total volume, followed by the high and low densities at, respectively, 33 and 12%. The fractions change only slightly at 290 K, with the values for the regions with normal, high, and low densities being, respectively, 59, 31, and 10%, with all the changes being well in the range of the numerical error. A summary of the density fluctuations in the nanotube is shown in Fig. 4. At $T = 230$ and 290 K, the low density represents the lowest portion, and there is a peak at around a density of about 0.925 g/cm,^{3} which closely matches the density of bulk water at the same temperature [59]. In contrast, at $T = 290$ K there is not a unique peak. Instead, the molecules with normal density have a broader distribution. Nevertheless, the fractions of the three types of local densities at 290 K in the larger nanotubes are significantly different. Higher volume fractions of the normal density, 63% in the (20,0) and 70% in the (30,0) nanotubes, are present. In contrast, the fractions of the regions with high density in the (20,0) and (30,0) nanotubes are only 28 and 23%. The low-density type also experiences such a decrease, which are 9 and 7%. The anisotropy produced by the confinement can be a possible explanation of the rheology, as explained below. Note that structural changes in sheared liquids have been interpreted as the fingerprint of non-Newtonian rheology [40].

C. Intermediate scattering function and the relaxation time

Figure 5 presents the ISF for bulk and confined waters. Note that in the MD simulations of water at low temperatures that we consider the bulk water does not freeze, because in order to produce ice one must add nucleation sites for ice; otherwise, it is very unlikely that MD simulation of bulk water at such temperatures can produce ice. In other words, one has to put the supercooled water in contact with, for example, hexagonal ice in order to produce the frozen state; see, for example, Naserifar and Goddard [81], who recently simulated supercooled bulk water without ice.

The relaxation times that were computed for bulk water at 230, 250, 270, and 290 K were, respectively, 60, 23, 12.5, and 6.9 ps. The corresponding values for confined water in the (12,0) nanotube at the same temperatures were 4.18, 2.08, 1.01, and 0.57 ns, respectively, about two orders of magnitude larger than those of bulk water. The fact that the relaxation times of confined water are much larger than those in the bulk provides evidence for the existence of a possible critical shear rate $\dot{\gamma}_c$ for non-Newtonian rheology. As mentioned earlier, one usually finds that $\dot{\gamma}_c$ for supercooled liquids is smaller than the inverse of the relaxation time, implying that $\dot{\gamma}_c$ is very small. Here, we present evidence indicating that the critical shear

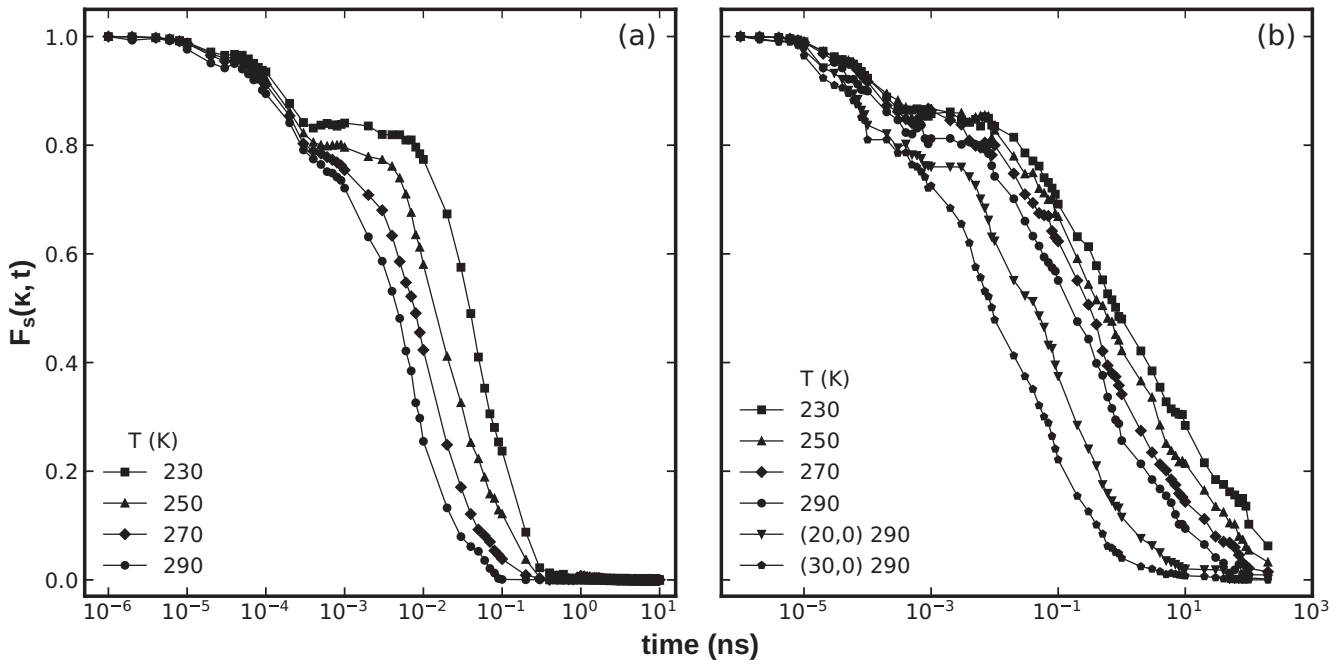

FIG. 5. The intermediate scattering function $F_s(\kappa, t)$ for (a) bulk water and (b) water confined in the nanotube.

rate of confined water is smaller than the corresponding value for the bulk water, implying that shear-thinning rheology in confinement sets in much earlier than in the bulk. We shall return to this point shortly.

D. Rheology

The viscosity of bulk supercooled water was computed by the NEMD simulation. The results are shown in Fig. 6. We note that the onset of non-Newtonian rheology occurs for shear rates between 10^9 and 10^{10} s^{-1}, which is about one order of magnitude lower than the inverse of the relaxation times. The effective zero shear rate viscosity of the water confined in the (12,0) nanotube was computed by the GK formalism. The results are shown in Fig. 7, and indicate that water in the nanotube is a very viscous fluid at 230 K. The viscosity decreases gradually as temperature rises.

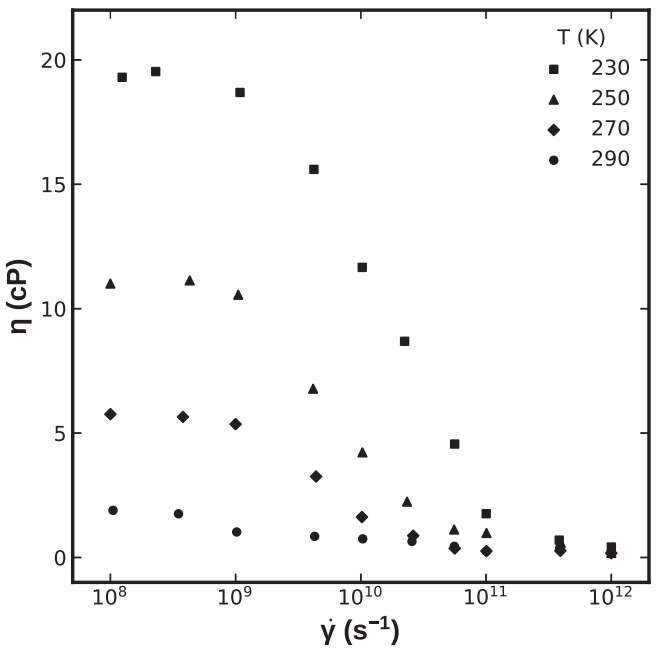

FIG. 6. Viscosity of bulk water as a function of the shear rate, computed by the NEMD simulation.

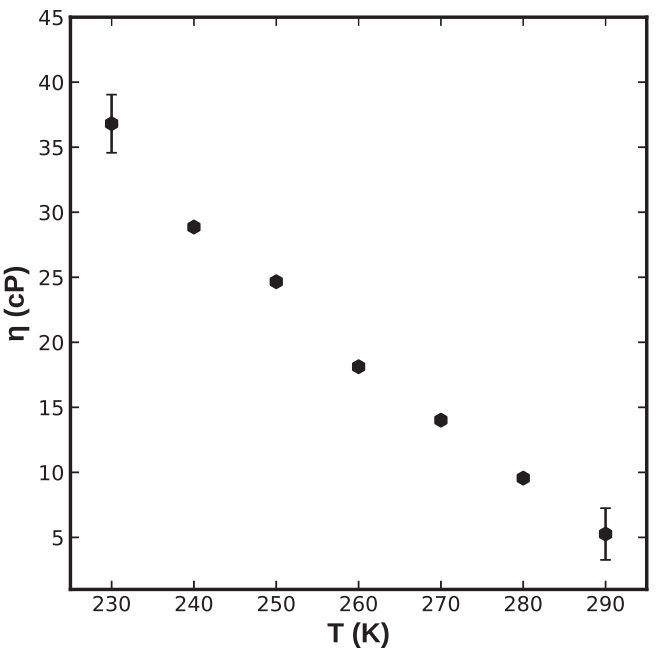

FIG. 7. Zero-shear rate viscosity of water in the nanotube, computed by the Green-Kubo equation.

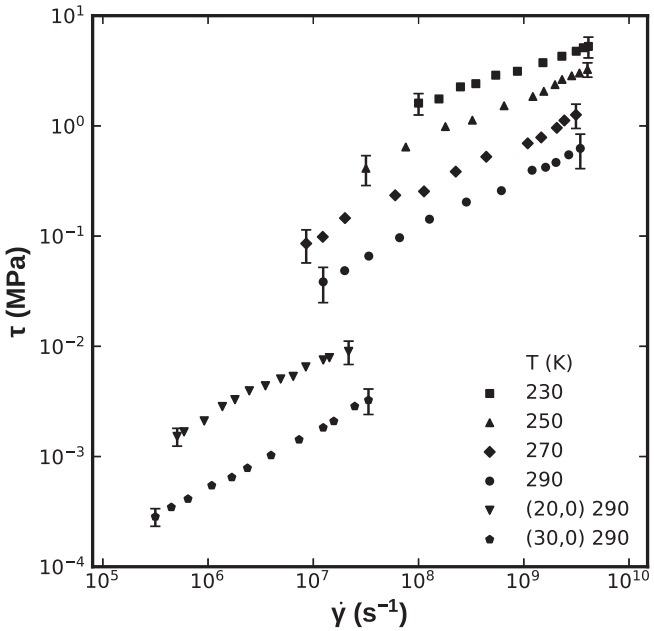

FIG. 8. Temperature and shear rate dependence of the shear stress in the nanotube, computed by the NEMD simulation.

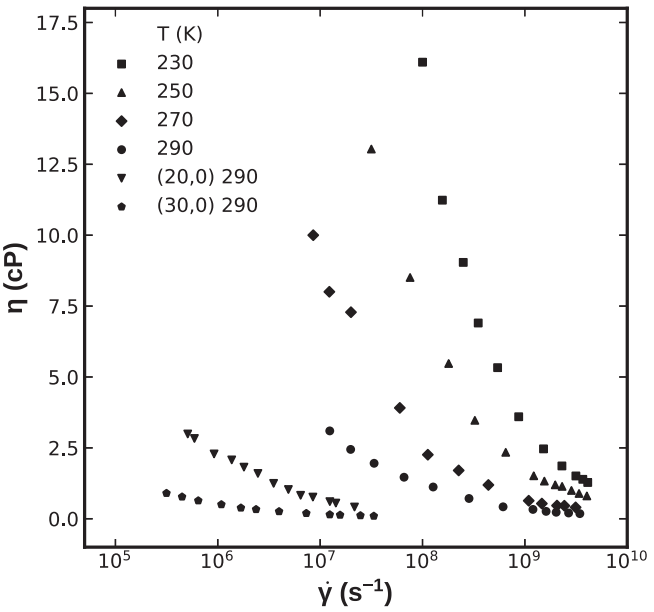

FIG. 9. Temperature and shear rate dependence of the effective viscosity of water, computed by the NEMD simulation. They indicate non-Newtonian rheology.

Zero shear rate viscosity of water at room temperature, computed by the GK relation, was also reported previously by us [28]. Our estimates are about twice larger than the experimental values reported for bulk supercooled water [82] over the same temperature range. Note that, as has also been pointed out by others [70,71], use of the GK relation in confined media is not without problems, because the equation was originally derived for homogeneous fluids. Moreover, the frequency of sampling and the periodicity may generate artifacts. Despite this, as explained below, the calculations based on the GK relation can still be useful.

To obtain more accurate estimates of the viscosity based on sound theoretical foundations, we also carried out a separate set of NEMD simulations to compute shear rate dependence of the effective viscosity. Figure 8 presents the shear stress–shear rate diagram for water in the nanotubes as a function of the temperature. In all cases the shear stress does not vary significantly with the shear rate $\dot{\gamma}$ when $\dot{\gamma}$ is small. But, as $\dot{\gamma}$ increases, so also does the shear stress. The results shown in Fig. 8 indicate clearly a non-Newtonian rheology at all temperatures.

To understand this better, as well as obtain more accurate estimates of water viscosity in the nanotube, we define an effective viscosity η by Eq. (4). For Newtonian fluids, η is independent of the shear rate and depends only on T (and pressure P) and the molecular structure of the solution, but for non-Newtonian fluids η depends also on $\dot{\gamma}$. The results for η, presented in Fig. 9, provide further evidence that the confinement and the supercooled state of water enhance the non-Newtonian rheology, and that water resembles a shear-thinning fluid since its viscosity decreases with the shear rate $\dot{\gamma}$. Note also that as the temperature and the nanotubes' diameter increase the dependence of η on $\dot{\gamma}$ weakens, hence indicating that rheology of water in the nanotube at temperatures higher than room temperature resembles increasingly that of Newtonian fluids.

We note that even though it is not possible to precisely determine the critical shear rate for confined water it is evident from Fig. 9 that it is at least two or three orders of magnitude smaller than the inverse of the relaxation times in the same systems. This indicates that shear-thinning rheology in nanotubes emerges earlier than in the bulk.

The effective viscosity for the smallest (zero) shear rate that we computed by the NEMD simulations in the nanotube is smaller than that computed by the GK formalism, but much closer to the experimental data [82] for supercooled water under bulk condition over the same temperature range. We explain this by noting that [83] thermal fluctuations of shear stress at equilibrium will be affected not only by the viscosity but also by the slip boundary condition at the wall, which is known to exist in flow through small nanotubes. Thus, because the GK equation was intended for homogeneous fluids, it does not take into account the slip on the walls.

Therefore, the GK provides *overestimates* of the effective viscosity in confined media. This implies that either the GK formulation must be modified in order to take into account the slip effect or the estimates that it provides for the effective viscosity of liquids in confined media with slip boundary conditions should be viewed as a sort of *upper bound* to the true values, as it ignores the slip on the walls. Indeed, recent research [84] has shown that for confined fluids between parallel plates the GK equation is inadequate for computing the viscosity.

Finally, we note that although the viscosities for the bulk and confined water were computed by different methods the differences between the relaxation times agree with the slow dynamics encountered due to confinement, which was reported previously in several studies [5–10,19].

IV. SUMMARY

This paper reported on a study of rheology of supercooled water in small nanotubes. We reported the results of extensive equilibrium and nonequilibrium molecular dynamics simulations of supercooled water in small SiCNTs over a wide range of temperatures. The properties computed, namely, the CCF, MSDs, $g(r)$, shear stress–shear rate diagram, and effective viscosity, indicate that not only does water not freeze at temperatures way below the bulk freezing temperature of 273 K but also regions with high and low densities coexist in the nanotube at such temperatures and above the freezing point. The volume fractions of the regions with locally high and low densities tend, however, to decrease as temperature and diameter of the nanotube increase. We also note that the non-Newtonian regime tends to be in a narrower range of shear rates as the nanotube's diameter increases. Moreover, while the presence of the liquid with different densities in smaller nanotubes is very clear, the same is not true in larger ones, where the non-Newtonian behavior is weaker.

We also reported clear evidence for non-Newtonian rheology of confined water over the same range of temperature at high velocities. We suspect that the existence and the relative abundance of the water with different local densities may be linked to the non-Newtonian rheology, since it has been shown that the structure of liquids has a strong relationship with their viscosity, especially in supercooled water [45]. Most recently, it was proposed [85] that water could behave as a polymer chain over certain time scales, which may provide further evidence for its non-Newtonian rheology in confinement.

These results may have important implications for flow of water and similar liquids in nanostructured materials, for biological systems, and for the design of devices for various medical applications at low temperatures.

ACKNOWLEDGMENTS

All the calculations were carried out using the computational resources of the Center for High Performance Computing at the University of Southern California. J.C.-R. acknowledges financial support from SENESCYT, Ecuador. Partial support of the work by the Petroleum Research Fund, administered by the American Chemical Society, is also gratefully acknowledged.

[1] J. Teixeira, Recent experimental aspects of the structure and dynamics of liquid and supercooled water, Mol. Phys. **110**, 249 (2012).

[2] V. Holten, C. E. Bertrand, M. A. Anisimov, and J. V. Sengers, Thermodynamics of supercooled water, J. Chem. Phys. **136**, 094507 (2012).

[3] F. Mallamace, C. Branca, M. Broccio, C. Corsaro, C.-Y. Mou, and S.-H. Chen, The anomalous behavior of the density of water in the range 30 K $< T <$ 373 K, Proc. Natl. Acad. Sci. USA **104**, 18387 (2007).

[4] C. A. Angell, R. D. Bressel, M. Hemmati, E. J. Sare, and J. C. Tucker, Water and its anomalies in perspective: Tetrahedral liquids with and without liquid-liquid phase transitions, Phys. Chem. Chem. Phys. **2**, 1559 (2000).

[5] G. S. Kell, Thermodynamic and transport properties of fluid water, in *The Physics and Physical Chemistry of Water. Water (A Comprehensive Treatise)*, edited by F. Frank (Springer, New York, 1972), Vol. 1, p. 363.

[6] Z. Mao and S. Sinnott, A computational study of molecular diffusion and dynamic flow through carbon nanotubes, J. Phys. Chem. B **104**, 4618 (2000).

[7] J. Marti and M. C. Gordillo, Temperature effects on the static and dynamic properties of liquid water inside nanotubes, Phys. Rev. E **64**, 021504 (2001).

[8] C. Dellago, M. Naor, and G. Hummer, Proton Transport Through Water-Filled Carbon Nanotubes, Phys. Rev. Lett. **90**, 105902 (2003).

[9] A. Kolesnikov, J.-M. Zanotti, C.-K. Loong, P. Thiyagarajan, A. Moravsky, R. Loutfy, and C. Burnham, Anomalously Soft Dynamics of Water in a Nanotube: A Revelation of Nanoscale Confinement, Phys. Rev. Lett. **93**, 035503 (2004).

[10] A. Striolo, The mechanism of water diffusion in narrow carbon nanotubes, Nano Lett. **6**, 633 (2006).

[11] B. Mukherjee, P. Maiti, C. Dasgupta, and A. K. Sood, Strong correlations and Fickian water diffusion in narrow carbon nanotubes, J. Chem. Phys. **126**, 124704 (2007).

[12] J. Ma, A. Michaelides, D. Alfe, L. Schimka, G. Kresse, and E. Wang, Adsorption and diffusion of water on graphene from first principles, Phys. Rev. B **84**, 033402 (2011).

[13] S. O. Diallo, Pore-size dependence and characteristics of water diffusion in slitlike micropores, Phys. Rev. E **92**, 012312 (2015).

[14] S. Nakaoka, Y. Yamaguchi, T. Omori, M. Kagawa, T. Nakajima, and H. Fujimura, Molecular dynamics analysis of the velocity slip of a water and methanol liquid mixture, Phys. Rev. E **92**, 022402 (2015).

[15] E. Mamontov, C. J. Burnham, S.-H. Chen, A. P. Moravsky, C.-K. Loong, N. De Souza, and A. Kolesnikov, Dynamics of water confined in single-and double-wall carbon nanotubes, J. Chem. Phys. **124**, 194703 (2006).

[16] T. Nanok, N. Artrith, P. Pantu, P. Bopp, and J. Limtrakul, Structure and dynamics of water confined in single-wall nanotubes, J. Phys. Chem. A **113**, 2103 (2009).

[17] L. Scalfi, G. Fraux, A. Boutin, and F.-X. Coudert, Structure and dynamics of water confined in imogolite nanotubes, Langmuir **34**, 6748 (2018).

[18] B. H. Mendona, D. N. de Freitas, M. H. Köhler, R. J. Batista, M. C. Barbosa, and A. B. de Oliveira, Diffusion behaviour of water confined in deformed carbon nanotubes, Physica A **517**, 491 (2019).

[19] P. Kumar, S. Buldyrev, F. Starr, N. Giovambattista, and H. E. Stanley, Thermodynamics, structure, and dynamics of water confined between hydrophobic plates, Phys. Rev. E **72**, 051503 (2005).

[20] D. Takaiwa, I. Hatano, K. Koga, and H. Tanaka, Phase diagram of water in carbon nanotubes, Proc. Natl. Acad. Sci. USA **105**, 39 (2008).

[21] K. Nomura, T. Kaneko, J. Bai, J. Francisco, K. Yasuoka, and X. Zeng, Evidence of low-density and high-density liquid phases and isochore end point for water confined to carbon nanotube, Proc. Natl. Acad. Sci. USA **114**, 4066 (2017).

[22] X.-Q. Chu, A. Kolesnikov, A. Moravsky, V. Garcia-Sakai, and S.-H. Chen, Observation of a dynamic crossover in water confined in double-wall carbon nanotubes, Phys. Rev. E **76**, 021505 (2007).

[23] M. Raju, A. Van Duin, and M. Ihme, Phase transitions of ordered ice in graphene nanocapillaries and carbon nanotubes, Sci. Rep. **8**, 3851 (2018).

[24] C. E. Bertrand, Y. Zhang, and S.-H. Chen, Deeply-cooled water under strong confinement: Neutron scattering investigations and the liquid-liquid critical point hypothesis, Phys. Chem. Chem. Phys. **15**, 721 (2013).

[25] S. O. Diallo, L. Vlcek, E. Mamontov, J. K. Keum, J. Chen, J. S. Hayes, Jr., and A. A. Chialvo, Translational diffusion of water inside hydrophobic carbon micropores studied by neutron spectroscopy and molecular dynamics simulation, Phys. Rev. E **91**, 022124 (2015).

[26] R. S. Singh, J. W. Biddle, P. G. Debenedetti, and M. Anisimov, A two-state thermodynamics and the possibility of a liquid-liquid phase transition in supercooled TIP4P/2005 water, J. Chem. Phys. **144**, 144504 (2016).

[27] M. Foroutan, S. M. Fatemi, and F. Shokouh, Graphene confinement effects on melting/freezing point and structure and dynamics behavior of water, J. Mol. Graphics Modell. **66**, 85 (2016).

[28] M. Khademi and M. Sahimi, Molecular dynamics simulation of pressure-driven water flow in silicon-carbide nanotubes, J. Chem. Phys. **135**, 204509 (2011).

[29] M. Khademi and M. Sahimi, Static and dynamic properties of supercooled water in small nanotubes, J. Chem. Phys. **145**, 024502 (2016).

[30] F. Mallamace, M. Broccio, C. Corsaro, A. Faraone, D. Majolino, V. Venuti, L. Liu, C.-Y. Mou, and S.-H. Chen, Evidence of the existence of the low-density liquid phase in supercooled, confined water, Proc. Natl. Acad. Sci. USA **104**, 424 (2007).

[31] J. Cobeña-Reyes, R. K. Kalia, and M. Sahimi, Complex behavior of ordered and icelike water in carbon nanotubes near its bulk boiling point, J. Phys. Chem. Lett. **9**, 4746 (2018).

[32] *Dynamics of Soft Matter: Neutron Applications*, edited by V. G. Sakai, C. Alba-Simionesco, and S.-H. Chen (Springer, New York, 2011).

[33] R. J. Mashl, S. Joseph, N. R. Aluru, and E. Jakobsson, Anomalously immobilized water: A new water phase induced by confinement in nanotubes, Nano Lett. **3**, 589 (2003).

[34] M. Khademi, R. K. Kalia, and M. Sahimi, Dynamics of supercooled water in nanotubes: Cage correlation function and diffusion coefficient, Phys. Rev. E **92**, 030301 (2015).

[35] C. Alba-Simionesco, B. Coasne, G. Dosseh, G. Dudziak, K. E. Gubbins, R. Radhakrishnan, and M. Sliwinska-Bartkowiak, Effects of confinement on freezing and melting, J. Phys.: Condens. Matter **18**, R15 (2006).

[36] B. Ramos-Alvarado, S. Kumar, and G. P. Peterson, Hydrodynamic slip in silicon nanochannels, Phys. Rev. E **93**, 033117 (2016).

[37] N. Wei, X. Peng, and Z. Xu, Breakdown of fast water transport in graphene oxides, Phys. Rev. E **89**, 012113 (2014).

[38] M. Shaat and Y. Zheng, Fluidity and phase transitions of water in hydrophobic and hydrophilic nanotubes, Sci. Rep. **9**, 5689 (2019).

[39] C. D. Lorenz, M. Chandross, J. M. D. Lane, and G. S. Grest, Nanotribology of water confined between hydrophilic alkylsilane selfassembled monolayers, Modell. Simul. Mater. Sci. Eng. **18**, 034005 (2010).

[40] A. Jabbarzadeh, P. Harrowell, and R. I. Tanner, Crystal Bridge Formation Marks the Transition to Rigidity in a Thin Lubrication Film, Phys. Rev. Lett. **96**, 206102 (2006).

[41] L. Ramin and A. Jabbarzadeh, Effect of water on structural and frictional properties of self assembled monolayers, Langmuir **29**, 13367 (2013).

[42] R. García Fernández, J. Abascal, and C. Vega, The melting point of ice Ih for common water models calculated from direct coexistence of the solid-liquid interface, J. Chem. Phys. **124**, 144506 (2006).

[43] J. S. Hub, B. L. de Groot, H. Grubmüller, and G. Groenhof, Quantifying artifacts in Ewald simulations of inhomogeneous systems with a net charge, J. Chem. Theory Comput. **10**, 381 (2014).

[44] D. Bostick and M. Berkowitz, The implementation of slab geometry for membrane channel molecular dynamics simulations, Biophys. J. **85**, 97 (2003).

[45] T. S. Ingebrigtsen and H. Tanaka, Structural predictor for nonlinear sheared dynamics in simple glass-forming liquids, Proc. Natl. Acad. Sci. USA **115**, 87 (2018).

[46] V. Lubchenko, Shear thinning in deeply supercooled melts, Proc. Natl. Acad. Sci. USA **106**, 11506 (2009).

[47] A. Furukawa, Onset of shear thinning in glassy liquids: Shear-induced small reduction of effective density, Phys. Rev. E **95**, 012613 (2017).

[48] D. Bai, Size, morphology and temperature dependence of the thermal conductivity of single-walled silicon carbide nanotubes, Fuller. Nanotub. Carbon Nanostruct. **19**, 271 (2011).

[49] B. Elyassi, M. Sahimi, and T. T. Tsotsis, A novel sacrificial interlayer-based method for the preparation of silicon carbide membranes, J. Membr. Sci. **316**, 73 (2008).

[50] K. Malek and M. Sahimi, Molecular dynamics simulations of adsorption and diffusion of gases in silicon-carbide nanotubes, J. Chem. Phys. **132**, 014310 (2010).

[51] S. H. Barghi, T. T. Tsotsis, and M. Sahimi, Hydrogen sorption hysteresis and superior storage capacity of silicon-carbide nanotubes over their carbon counterparts, Int. J. Hydrogen Energy **39**, 21107 (2014).

[52] S. H. Barghi, T. T. Tsotsis, and M. Sahimi, Experimental investigation of hydrogen adsorption in doped silicon-carbide nanotubes, Int. J. Hydrogen Energy **41**, 369 (2016).

[53] A. J. Rosenbloom, D. M. Sipe, Y. Shishkin, Y. Ke, R. P. Devaty, and W. J. Choyke, Nanoporous SiC: A candidate semi-permeable material for biomedical applications, Biomed. Microdevices **6**, 261 (2004).

[54] S. J. Mahdizadeh and E. K. Goharshadi, Natural gas storage on silicon, carbon, and silicon carbide nanotubes: A combined quantum mechanics and grand canonical Monte Carlo simulation study, J. Nanopart. Res. **15**, 1393 (2013).

[55] A. Mavrandonakis, G. E. Froudakis, M. Schnell, and M. Mühlhäuser, From pure carbon to silicon-carbon nanotubes: An *ab-initio* study, Nano Lett. **3**, 1481 (2003).

[56] I.-C. Yeh and G. Hummer, System-size dependence of diffusion coefficients and viscosities from molecular dynamics simulations with periodic boundary conditions, J. Phys. Chem. B **108**, 15873 (2004).

[57] M. Menon, E. Richter, A. Mavrandonakis, G. Froudakis, and A. N. Andriotis, Structure and stability of SiC nanotubes, Phys. Rev. B **69**, 115322 (2004).

[58] J. Abascal, E. Sanz, R. García Fernández, and C. Vega, A potential model for the study of ices and amorphous water: TIP4P/Ice, J. Chem. Phys. **122**, 234511 (2005).

[59] V. Holten and M. A. Anisimov, Entropydriven liquid-liquid separation in supercooled water, Sci. Rep. **2**, 713 (2012).

[60] D. J. Evans and G. P. Morriss, Nonlinearresponse theory for steady planar Couette flow, Phys. Rev. A **30**, 1528 (1984).

[61] R. H. A. Kohlrausch, Theorie des elektrischen Ruckstandes in der Leidner Flasche, Ann. Phys. Chem. (Poggendorff) **167**, 56 (1854).

[62] G. Williams and D. C. Watts, Non-symmetrical dielectric relaxation behaviour arising from a simple empirical decay function, Trans. Faraday Soc. **66**, 80 (1970).

[63] J. Tersoff, Modeling solid-state chemistry: Interatomic potentials for multicomponent systems, Phys. Rev. B **39**, 5566 (1989).

[64] H. Shen, Thermal-conductivity and tensile-properties of BN, SiC and Ge nanotubes, Comput. Mater. Sci. **47**, 220 (2009).

[65] A. R. Setoodeh, M. Jahanshahi, and H. Attariani, Atomistic simulations of the buckling behavior of perfect and defective silicon carbide nanotubes, Comput. Mater. Sci. **47**, 388 (2009).

[66] Y. Zhang and H. Huang, Stability of single-wall silicon carbide nanotubes: Molecular dynamics simulations, Comput. Mater. Sci. **43**, 664 (2008).

[67] F. Memarian, Ab. Fereidoon, S. Khodaei, A. Mashhadzadeh, and M. Davish Ganji, Molecular dynamic study of mechanical properties of single/double wall SiCNTs: Consideration temperature, diameter and interlayer distance, Vacuum **139**, 93 (2017).

[68] E. Rabani, J. Gezelter, and B. J. Berne, Direct Observation of Stretched-Exponential Relaxation in Low-Temperature Lennard-Jones Systems using the Cage Correlation Function, Phys. Rev. Lett. **82**, 3649 (1999).

[69] X. Chen, G. Cao, A. Han, V. Punyamurtula, L. Liu, P. Culligan, T. Kim, and Y. Qiao, Nanoscale fluid transport: Size and rate effects, Nano Lett. **8**, 2988 (2008).

[70] B. Xu, Y. Li, T. Park, and X. Chen, Effect of wall roughness on fluid transport resistance in nanopores, J. Chem. Phys. **135**, 144703 (2011).

[71] L. Liu, L. Zhang, Z. Sun, and G. Xi, Graphene nanoribbon-guided fluid channel: A fast transporter of nanofluids, Nanoscale **4**, 6279 (2012).

[72] A. M. Kheirabadi, A. Moosavi, and A. M. Akbarzadeh, Nanofluidic transport inside carbon nanotubes, J. Phys. D **47**, 065304 (2014).

[73] B. Liu, R. Wu, J. Baimova, H. Wu, A. Law, S. Dmitriev, and K. Zhou, Molecular dynamics study of pressure-driven water transport through graphene bilayers, Phys. Chem. Chem. Phys. **18**, 1886 (2016).

[74] B. Liu, R. Wu, A. Law, X. Feng, L. Bai, and K. Zhou, Channel morphology effect on water transport through graphene bilayers, Sci. Rep. **6**, 38583 (2016).

[75] R. W. Hockney and J. W. Eastwood, *Computer Simulation Using Particles* (CRC Press, Boca Raton, FL, 1988).

[76] J.-P. Ryckaert, G. Ciccotti, and H. Berendsen, Numerical integration of the cartesian equations of motion of a system with constraints: Molecular dynamics of *n*-alkanes, J. Comput. Phys. **23**, 327 (1977).

[77] S. Plimpton, Fast parallel algorithms for short-range molecular dynamics, J. Comput. Phys. **117**, 1 (1995).

[78] W. Humphrey, A. Dalke, and K. Schulten, VMD: Visual molecular dynamics, J. Mol. Graphics **14**, 33 (1996).

[79] P. B. Louden and J. D. Gezelter, Why is ice slippery? Simulations of shear viscosity of the quasi-liquid layer on ice, J. Phys. Chem. Lett. **9**, 3686 (2018).

[80] V. Weiss, M. Rullich, C. Köhler, and T. Frauenheim, Kinetic aspects of the thermostatted growth of ice from supercooled water in simulations, J. Chem. Phys. **135**, 034701 (2011).

[81] S. Naserifar and W. A. Goddard III, Anomalies in supercooled water at 230 K arise from a 1D polymer to 2D network topological transformation, J. Phys. Chem. Lett. **10**, 6267 (2019).

[82] A. Dehaoui, B. Issenmann, and F. Caupin, Viscosity of deeply supercooled water and its coupling to molecular diffusion, Proc. Natl. Acad. Sci. USA **112**, 12020 (2015).

[83] A. Zaragoza, M. A. Gonzalez, L. Joly, I. López-Montero, M. A. Canales, A. L. Benavides, and C. Valeriani, Molecular dynamics study of nanoconfined TIP4P/2005 water: How confinement and temperature affect diffusion and viscosity, Phys. Chem. Chem. Phys. **21**, 13653 (2019).

[84] J. de la Torre, D. Duque-Zumajo, D. Camargo, and P. Español, Microscopic Slip Boundary Conditions in Unsteady Fluid Flows, Phys. Rev. Lett. **123**, 264501 (2019).

[85] S. Naserifar and W. A. Goddard III, Liquid water is a dynamic polydisperse branched polymer, Proc. Natl. Acad. Sci. USA **116**, 1998 (2019).